

cytometric analysis of CD31, CD45 and VEGFR2 expression in early EPCs and late EPCs derived from cord blood (Fig. 1C). Similar to the immunocytochemical staining, the expression of CD45 in late EPC was weaker than that in early EPCs, while VEGFR2 expression in late EPCs was stronger than that in early EPCs. CD14 expression was observed only in early EPCs (data not shown).

Tubular structures could be constructed by late EPC, but not by early EPC

To assess the tube-forming activities of early and late EPCs, both cell types were analyzed by a novel method which promoted capillary formation *in vitro*. Early EPCs, late EPCs and HUVECs were distributed linearly on a specific substrate

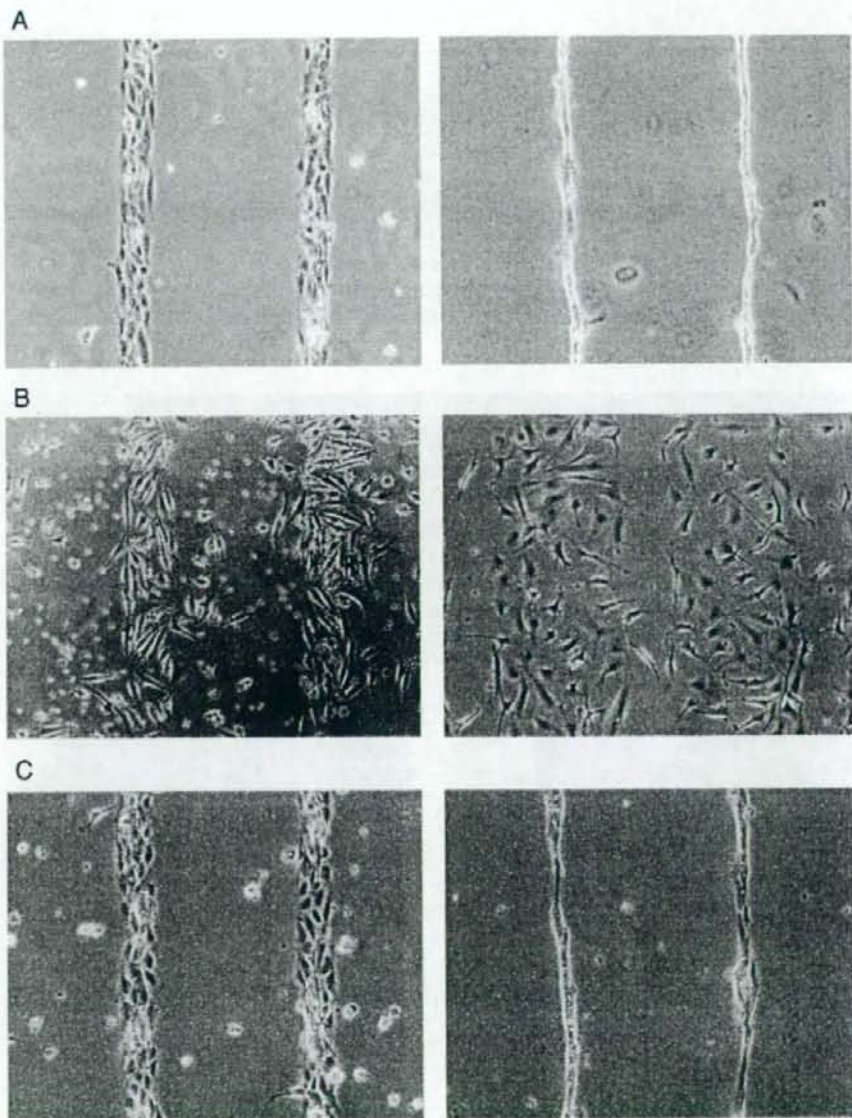


Fig. 2 - Tube forming activities in early and late EPCs compared with HUVECs. Cells (2×10^5) were seeded on the glass substrate and cultured for 18 h (A-C, left), then transplanted to Matrigel. Twenty-four hours after transplantation (right), HUVECs formed tubular structures (A). Early EPCs spread on Matrigel and did not form tubular structures (B). Late EPCs formed tubular structures (C).

(Fig. 2, left) and were subsequently transferred to Matrigel (Fig. 2, right). During the transfer of patterned cells to Matrigel, HUVECs changed cellular morphology to form capillary-like structures. Twenty-four hours after cell transfer, the substrate was removed and tubular structures were readily observed by a light microscopy (Fig. 2A). Electron microscopic observation revealed that the luminal structure consisted of four to five HUVECs [22]. In contrast, linearly

arrayed early EPCs did not form tubular structures (Fig. 2B). The time course of tube formation in late EPCs was quite similar to that in HUVECs (Fig. 2C).

After HUVECs or late EPC were loaded with calcein-AM, the tubular structures were assessed with a laser confocal microscope. The luminal structure formed by late EPCs was observed as well as that by HUVECs (Figs. 3A, B). When tubes formed by HUVECs and late EPCs were stained for VE-

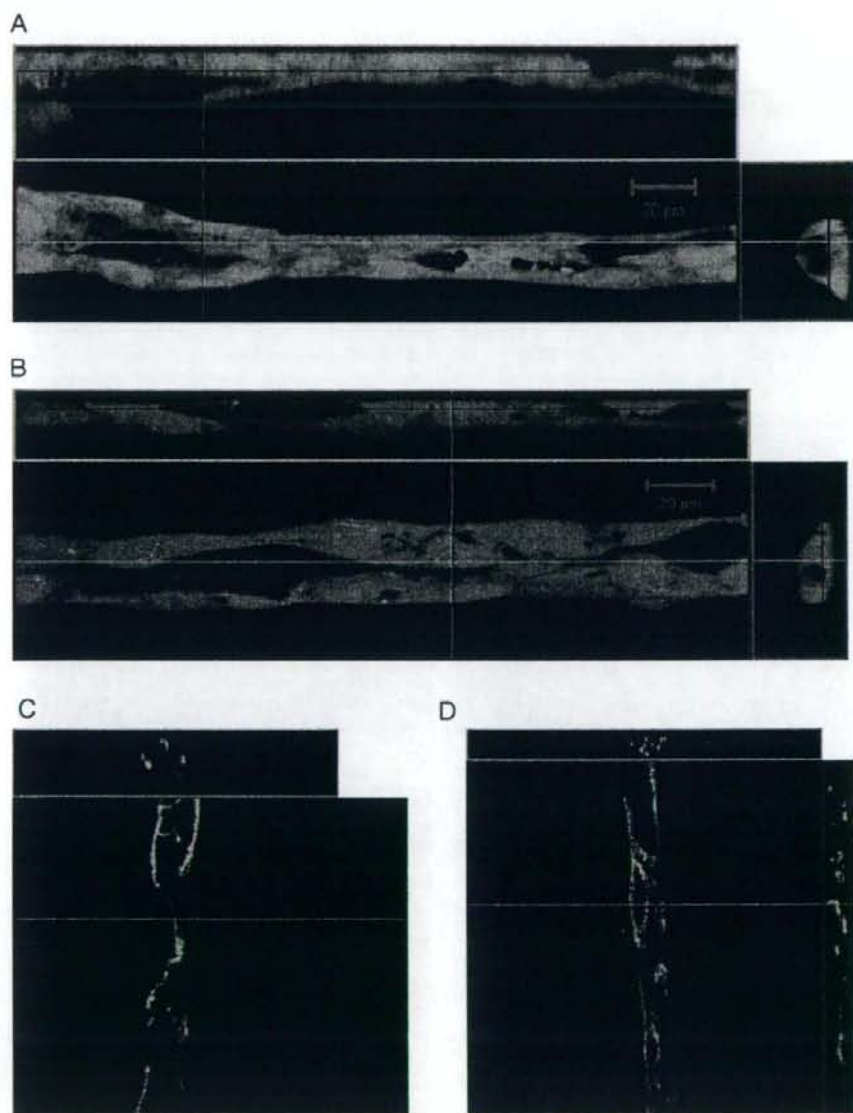


Fig. 3 - Three-dimensional images of tubular structures formed by HUVECs and late EPCs. Tubular structures formed by HUVECs (A) and late EPCs (B) were stained with calcein-AM. The luminal structure was observed with a laser confocal microscope. Scale bar = 20 μ m. Immunostaining of HUVEC (C) and late EPCs (D) tubular structures with anti-VE-cadherin. The localization of VE-cadherin was observed at cell-cell junctions.

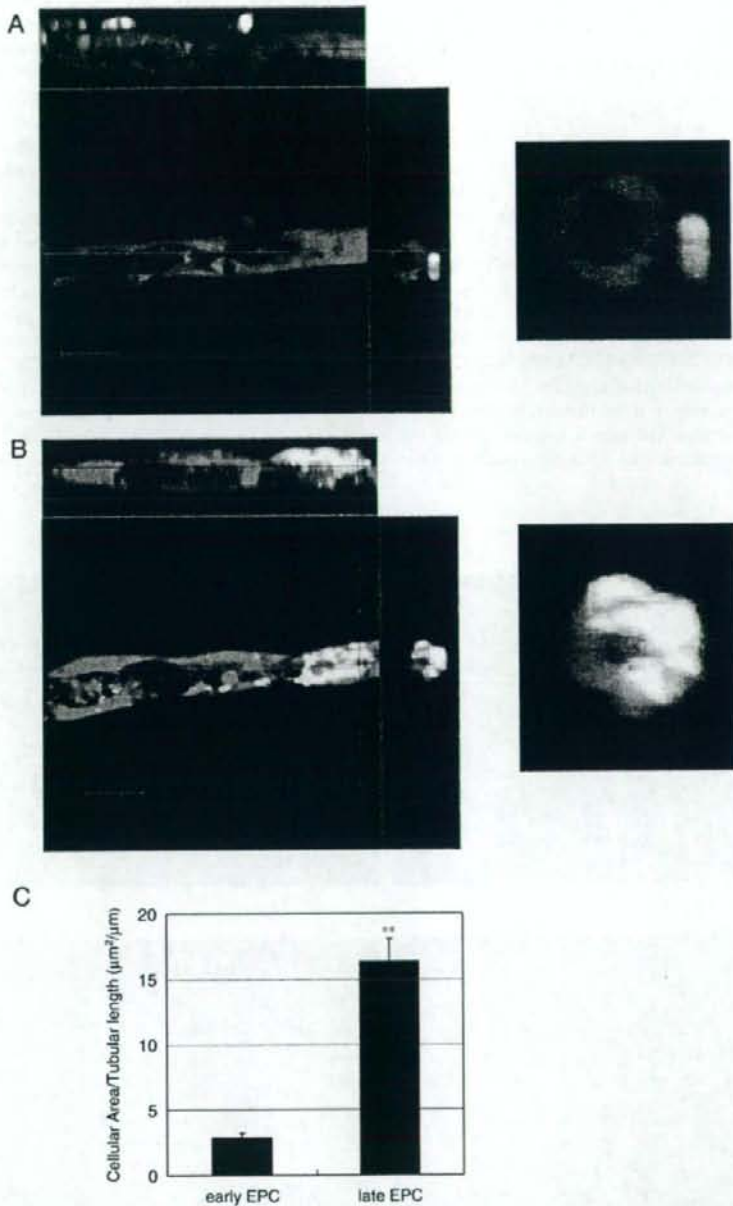


Fig. 4 - Cooperative tube-forming activity of EPCs and HUVECs. After early or late EPCs were stained with PKH26 Red, EPCs and HUVECs were mixed and co-cultured on the substrate, and then transplanted to Matrigel. The ratio of EPCs to HUVECs was 1:10. (A) Tubular structures formed by these EPCs and HUVECs were then labeled with Calcein-AM. Tubular structure constructed with both early EPCs (yellow) and HUVECs (green). Tubular structures were observed three dimensionally with a laser confocal microscopy. The early EPCs attached to the tube surface and were not incorporated into the tubular structure formed by HUVECs. Scale bar = 20 μm . (B) Tubular structure constructed with both late EPCs (yellow) and HUVECs (green). The late EPCs participated in tube formation with HUVECs. Scale bar = 20 μm . (C) The incorporation of EPCs into tube structure was calculated by the area of EPC in the indicated length of tubular structure. Value is the mean and SE (standard error) of 30. ** $P < 0.01$ vs. early EPCs.

cadherin, a specific endothelial cell-cell adhesion molecule, we observed VE-cadherin at cell-cell junctions (Figs. 3C, D).

Late EPCs, but not early EPCs, participated in tube formation with HUVECs

When EPCs are mixed with HUVECs and incubated on Matrigel, EPCs are incorporated into the tubular structure formed by HUVECs [5]. To confirm this, early EPCs or late EPCs were mixed with HUVECs and they were applied to the same tube formation systems. To distinguish the EPCs from HUVECs, the EPCs were labeled with PKH26 Red. Tubular structures formed by these EPCs and HUVECs were then labeled with Calcein-AM. The fluorescence of EPC and HUVECs was observed with a laser confocal microscopy. The early EPC as well as the late EPCs were observed in the tubular structure. However, by a three-dimensional imaging, we demonstrated that the early EPCs were only attached to the tube surface and were not incorporated into the tube structure formed by HUVECs (Fig. 4A). In contrast, the late EPCs participated in tube

formation with HUVECs (Fig. 4B). To quantify the incorporation of EPCs into tube structure was calculated by the area of EPC per the indicated length of tubular structure. The incorporation of late EPCs into tubular structures was over 5-fold larger than that of early EPCs (Fig. 4C).

Late EPCs integrated into pre-existing tubular structures formed by HUVECs while early EPCs caused tubular sprouting

In order to investigate whether EPCs could substitute for HUVECs in preformed tubular structures, EPCs and HUVECs were independently cultured. HUVECs labeled with PKH26 Red were seeded onto the substrate and EPCs labeled with PKH26 Green were suspended in Matrigel. The patterned HUVECs on the substrate were transferred to the EPC-containing Matrigel. The late EPCs migrated toward the tubular structures and were observed adjacent after 6 h (Fig. 5A) and attached to the tubes 10 h later (Fig. 5B). Thereafter, they were incorporated into the tubular structure 24 h later (Fig. 5C). In contrast, early EPCs did not migrate toward the tubes and were not

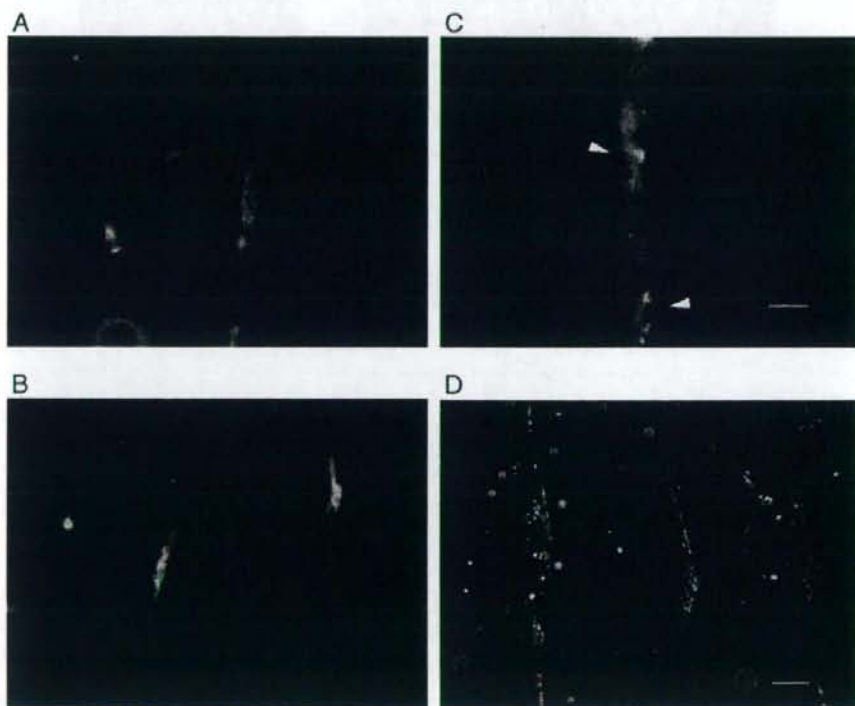


Fig. 5 – Incorporation of EPCs into preformed tubular structures. HUVECs labeled with PKH26 Red were seeded on the substrate and EPCs labeled with PKH26 Green were suspended in Matrigel. The patterned HUVECs on the substrate were transferred to the EPC-containing Matrigel. (A) Six hours after transplantation, late EPCs were migrating toward the tubular structure preformed by HUVECs. (B) Ten hours after transplantation, late EPCs were attached to the tube. (C) Twenty-four hours after transplantation, late EPCs were incorporated into the tubular structure preformed by HUVECs (yellow arrow heads). Scale bar = 30 μ m. (D) Twenty-four hours after transplantation, early EPCs had not been incorporated into the tubular structure preformed by HUVECs. The HUVECs in the tubular structure were sprouting and migrating. Scale bar = 100 μ m.

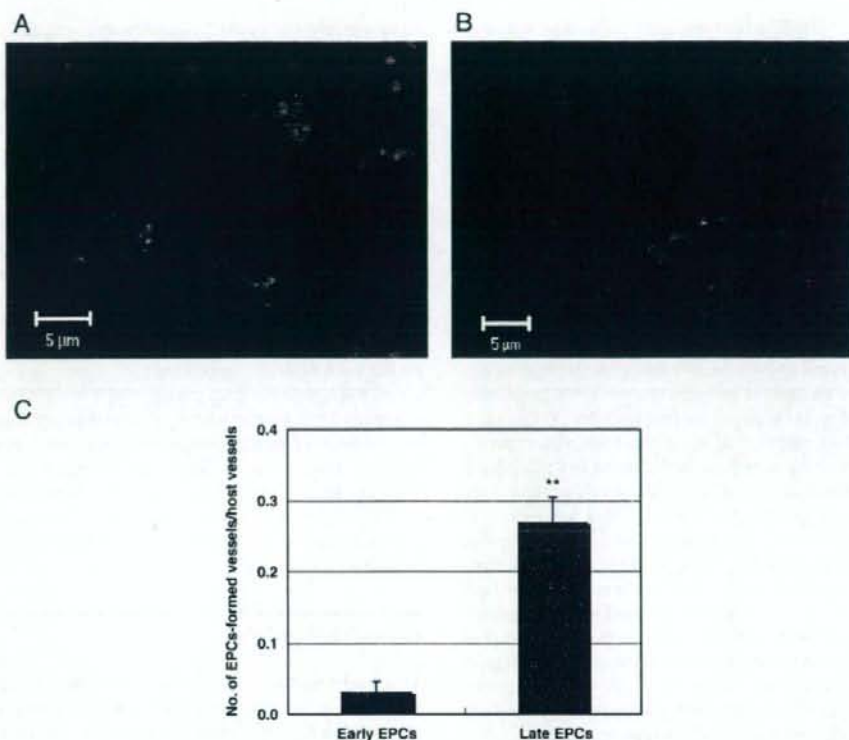


Fig. 6 – *In vivo* angiogenesis assay. After occlusion of murine auricular vessel, early (A) or late (B) EPCs labeled with PKH26 Red were subcutaneously injected into the occluded pinna. Forty-eight hours after the cell injection, the mice were given BS1-lectin (green) intravenously and sacrificed. Scale bar = 5 μ m. (C) The numbers of blood vessels derived from each EPCs observed in 5 sections were normalized to the number of recipient blood vessels. The data are shown as the mean and SE of three mice and data are mean of 5 fields/mouse. ** $P < 0.01$ vs. early EPCs.

incorporated during the observation period. However, after HUVECs were transferred to Matrigel containing early EPCs, the HUVECs in the tubular structures initiated sprouting and migrated toward early EPCs as evidenced by branching patterns between the tubular structures (Fig. 5D).

In vivo angiogenesis assay

To confirm the tube forming activity of each EPCs *in vivo*, the vessels derived from implanted EPCs were observed in the ear vessel occlusion model, early or late EPCs labeled with PKH26 Red were injected into the occluded pinna. Blood vessels derived from the late EPCs were observed in the pinna, but only a few blood vessels derived from early EPCs were observed (Fig. 6).

Discussion

We investigated the tube-forming capacity of early EPCs and late EPCs isolated from human peripheral blood and umbilical cord blood, respectively. In the previous report, it was

demonstrated that late EPCs were enriched in umbilical cord blood compared with adult peripheral blood [23]. Therefore, we isolated late EPCs from human umbilical cord blood. We used our novel method for capillary engineering which makes use of photo-catalytic lithography. Traditional assays for assessing characteristics of tube formation *in vitro* have been carried out by cultivation of endothelial cells in type I collagen and Matrigel. However, these methods could not distinguish between tube formation and morphological changes in the cells. The luminal structure of the vascular tube made in our present method was confirmed by an electron microscopy, a confocal laser microscopy and dye microinjection [22]. This technique is unique because the method allows one to focus on the process of tube formation. In contrast, tube formation in collagen and Matrigel evaluates the total activity of endothelial cells including migration, invasion and tube formation [24]. Using this novel method, we demonstrated that late EPCs participated in the formation of tubular structures with mature endothelial cells, i.e., HUVECs. It is interesting that late EPCs migrated toward and adjacent to pre-existing tubular structures and finally were incorporated

into the structure itself. In contrast, early EPCs could not form tubular structures, and they induced migration and sprouting of HUVECs present in the tubular structure. In a previous study using Matrigel, Hur et al. [18] demonstrated that early EPCs were incorporated into tubules when co-cultured with HUVECs, although the formation was weaker than that of late EPCs. However, that paper demonstrated the incorporation of EPCs into network structures of HUVECs on Matrigel, but could not show the incorporation of EPCs in tubular structures.

Our results showed that early EPCs were not capable of constructing tubular luminal structures even when they were co-cultured with mature endothelial cells. Instead, they stimulated the migration and sprouting of HUVECs from the tubular structure. These phenomena may be interpreted by the release of some growth factors from early EPCs. In our experiment, the amount of secreted interleukin-8 from early EPCs was significantly higher than that from late EPCs (0.81 ± 0.07 vs. 0.44 ± 0.02 , ng/ml, $P < 0.01$). It has been also reported that early EPCs secrete angiogenic factors such as VEGF [18,21], hepatocyte growth factor (HGF), and granulocyte-colony stimulating factor (G-CSF) [21]. These factors are known to stimulate endothelial cell migration and proliferation. In vivo experiments, implanted late EPCs in the occlusion tissues cause to construct new blood vessels by themselves, but early EPC could not. This result may be discussed with a hierarchy of EPCs [23]. It has been also reported that the different types of cells derived from peripheral blood have distinct actions in healing activity [25]. In this study, we demonstrated specific and distinct behaviors of early and late EPCs in tube formation and how they affected mature ECs in tube formation.

Although numerous reports have demonstrate that early EPCs have the potential to construct new blood vessels by themselves [5,6], some studies argued that early EPCs were not actually incorporated into newly formed vessels [26,27]. This discrepancy may be due to marked heterogeneity of EPCs used in their experiments. Numerous studies have fractionated EPC by phenotypic markers such as CD34, CD133, and VEGFR2 and various methods of EPCs isolation have been reported [5,6,28,29]. Among them CD34 has been often used for the marker of EPCs. However, Romagnani et al. showed that CD14 positive MNC-derived EPCs, which had been fractionated as CD34 negative, express very low level of CD34 using an antibody-conjugated magnetofluorescent liposomes (ACMFL) technique [30]. From these results, they suggested that CD14⁺CD34^{low} cells are the major source of early EPCs obtained from human peripheral blood MNC. This subset exhibited clonogenicity and multipotency to differentiate not only into endothelial cells, but also into osteocytes, or neural cells [30]. This report suggests that it is difficult to sort EPCs into highly defined fractions by ordinary FACS technique. In fact, each EPC population in previous studies is supposed to have a different phenotype even from the same source. To avoid these complexities, we collected and isolated early and late EPCs by focusing on their characteristics such as morphologies and proliferation pattern, and compared their tube-forming activities in short duration *in vitro* assays.

While the regenerative potential of EPCs has been demonstrated in animal models of myocardial and limb ischemia, the number of EPC available for transplantation is very important for cell-based therapy. Because EPCs are derived from a

limited endogenous pool, it is necessary to expand the number of EPCs *in vitro* or modulate phenotypes of EPCs. Iwaguro et al. reported that VEGF gene transfer in EPCs stimulated neovascularization in an *in vivo* model [31]. Murasawa et al. demonstrated that gene transfer of human telomerase reverse transcriptase into EPCs enhanced their angiogenic properties, mitogenic and migratory activities, and cell survival [32]. From the standpoint of cellular proliferation and phenotypic stability, late EPCs are superior to early EPCs. Therefore, the use of late EPCs for tissue engineering has been challenged [33–35]. With our method of generating transplantable capillary networks, the formation of tubular structures *in vitro* is a necessary precondition. The data presented here are thus important since the results demonstrate that late EPCs are a candidate for tissue engineering.

In conclusion, our data provide the first definitive evidence that early EPCs promote angiogenesis through migration and proliferation of mature endothelial cells, whereas late EPCs can form blood vessels. These results suggest that early EPCs and late EPCs have different roles in neovascularization *in vivo*. Finally, we expect that the novel culture system using a patterned substrate might be useful for future *in vitro* analyses of neovascularization.

Acknowledgments

This work was supported in part by research grants, 17209058, 1752342, the 21st Century COE Program from the Japan Society for the Promotion of Science, and KH31031 from Human Science Foundation, Tokyo, Japan. We thank Dai Nippon Printing Co. Ltd (Tokyo, Japan) for their kind preparation of substrate.

REFERENCES

- P.K.Y. Goon, C.J. Boos, C.Y.H. Lip, Circulating endothelial cells: markers of vascular dysfunction, *Clin. Lab.* 51 (2005) 531–538.
- N. Werner, S. Kosiol, T. Schiegl, P. Ahlers, K. Walenta, A. Link, M. Bohm, G. Nickenig, Circulating endothelial progenitor cells and cardiovascular outcomes, *N. Engl. J. Med.* 353 (2005) 999–1007.
- S. Rafii, D. Lyden, R. Benezra, K. Hattori, B. Heissig, Vascular and hematopoietic stem cells: novel targets for anti-angiogenesis therapy? *Nat. Rev. Cancer* 2 (2002) 826–835.
- W. Suh, K.L. Kim, J.M. Kim, I.S. Shin, Y.S. Lee, J.Y. Lee, H.S. Jang, J.S. Lee, J. Byun, J.H. Choi, E.S. Jeon, D.K. Kim, Transplantation of endothelial progenitor cells accelerates dermal wound healing with increased recruitment of monocytes/macrophages and neovascularization, *Stem Cells* 23 (2005) 1571–1588.
- T. Asahara, T. Murohara, A. Sullivan, M. Silver, R. van der Zee, T. Li, B. Witzensbichler, G. Schatterman, Isner, Isolation of putative progenitor endothelial cells for angiogenesis, *Science* 275 (1997) 964–967.
- T. Takahashi, C. Kalka, H. Masuda, D. Chen, M. Silver, M. Kearney, M. Wagner, J.M. Isner, T. Asahara, Ischemia- and cytokine-induced mobilization of bone marrow derived endothelial progenitor cells for neovascularization, *Nat. Med.* 5 (1999) 434–438.
- T. Asahara, H. Masuda, T. Takahashi, C. Kalka, C. Pastore, M. Silver, M. Kearney, M. Wagner, J.M. Isner, Bone marrow

- origin of endothelial progenitor cells responsible for postnatal vasculogenesis in physiological and pathological neovascularization, *Circ. Res.* 85 (1999) 221-228.
- [8] C. Kalk, H. Masuda, T. Takahashi, W.M. Kalka-Moll, M. Silver, M. Kearney, T. Li, J.M. Isner, T. Asahara, Transplantation of ex vivo expanded endothelial progenitor cells for therapeutic neovascularization, *Proc. Natl. Acad. Sci. U. S. A.* 97 (2000) 3422-3427.
- [9] T. Murohara, H. Ikeda, J. Duan, S. Shintani, K. Sasaki, H. Eguchi, I. Onitsuka, K. Matsui, T. Imaizumi, Transplanted cord blood-derived endothelial precursor cells augment postnatal neovascularization, *J. Clin. Invest.* 105 (2000) 1527-1536.
- [10] M. Hristov, W. Erl, P.C. Weber, Endothelial progenitor cells: mobilization, differentiation, and homing, *Arterioscler. Thromb. Vasc. Biol.* 23 (2003) 1185-1189.
- [11] E. Tateishi-Yuyama, H. Matsubara, T. Murohara, U. Ikeda, S. Shintani, H. Masaki, K. Armano, Y. Kishimoto, K. Yoshimoto, H. Akashi, K. Shimada, T. Iwasaka, T. Imaizumi, Therapeutic angiogenesis using cell transplantation (TACT) study investigators, therapeutic angiogenesis for patients with limb ischaemia by autologous transplantation of bone-marrow cells: a pilot study and a randomised controlled trial, *Lancet* 360 (2002) 427-435.
- [12] F.A. Kudo, T. Nishibe, M. Nishibe, K. Yasuda, Autologous transplantation of peripheral blood endothelial progenitor cells (CD34+) for therapeutic angiogenesis in patients with critical limb ischemia, *Int. Angiol.* 4 (2003) 344-348.
- [13] S. Shintani, T. Murohara, H. Ikeda, T. Ueno, T. Honma, A. Katoh, K. Sasaki, T. Shimada, Y. Oike, T. Imaizumi, Mobilization of endothelial progenitor cells in patients with acute myocardial infarction, *Circulation* 103 (2001) 2776-2779.
- [14] B. Assmus, V. Schachinger, C. Teupe, M. Britten, R. Lehmann, N. Dobert, F. Grunwald, A. Aicher, C. Urbich, H. Martin, D. Hoelzer, S. Dimmeler, A.M. Zeiher, Transplantation of progenitor cells and regeneration enhancement in acute myocardial infarction (TOPCARE-AMI), *Circulation* 106 (2002) 3009-3017.
- [15] M.B. Britten, N.D. Abolmaali, B. Assmus, R. Lehmann, J. Honold, J. Schmitt, T.J. Vogl, H. Martin, V. Schachinger, S. Dimmeler, A.M. Zeiher, Infarct remodeling after intracoronary progenitor cell treatment in patients with acute myocardial infarction (TOPCARE-AMI): mechanistic insights from serial contrast-enhanced magnetic resonance imaging, *Circulation* 108 (2003) 2212-2218.
- [16] Y. Lin, D.J. Weisdorf, A. Solovey, R.P. Heibel, Origins of circulating endothelial cells and endothelial outgrowth from blood, *J. Clin. Invest.* 105 (2000) 71-77.
- [17] R. Gulati, D. Jevremovic, T.E. Peterson, S. Chatterjee, V. Shah, R.G. Vile, R.D. Simari, Diverse origin and function of cells with endothelial phenotype obtained from adult human blood, *Circ. Res.* 93 (2003) 1023-1025.
- [18] J. Hur, C.H. Yoon, H.S. Kim, J.H. Choi, K.K. Hwang, B.H. Oh, M.M. Lee, Y.B. Park, Characterization of two types of endothelial progenitor cells and their different contributions to neovascularization, *Arterioscler. Thromb. Vasc. Biol.* 24 (2004) 288-293.
- [19] C.H. Yoon, J. Hur, K.W. Park, J.H. Kim, C.S. Lee, I.Y. Oh, T.Y. Kim, H.J. Cho, H.J. Kang, I.H. Chae, H.K. Yang, B.H. Oh, Y.B. Park, H.S. Kim, Synergistic neovascularization by mixed transplantation of early endothelial progenitor cells and late outgrowth endothelial cells: the role of angiogenic cytokines and matrix metalloproteinases, *Circulation* 112 (2005) 1618-1627.
- [20] C. Urbich, C. Heeschen, A. Aicher, E. Dernbach, A.M. Zeiher, S. Dimmeler, Relevance of monocytic features for neovascularization capacity of circulating endothelial progenitor cells, *Circulation* 108 (2003) 2511-2516.
- [21] J. Rehman, J. Li, C.M. Orschell, K.L. March, Peripheral blood "endothelial progenitor cells" are derived from monocyte/macrophages and secrete angiogenic growth factors, *Circulation* 107 (2003) 1164-1169.
- [22] A. Kobayashi, H. Miyake, H. Hattori, R. Kuwana, Y. Hiruma, K. Nakahama, S. Ichinose, M. Ota, M. Nakamura, S. Takeda, I. Morita, In vitro formation of capillary networks using optical lithographic techniques, *Biochem. Biophys. Res. Commun.* 358 (2007) 692-697.
- [23] D.A. Ingram, L.E. Mead, H. Tanaka, V. Meade, A. Fenoglio, K. Mortell, K. Pollok, M.J. Ferkowicz, D. Gilley, M.C. Yoder, Identification of a novel hierarchy of endothelial progenitor cells using human peripheral and umbilical cord blood, *Blood* 104 (2004) 2752-2760.
- [24] T.J. Lawley, Y. Kubota, Induction to morphologic differentiation of endothelial cells in culture, *J. Invest. Dermatol.* 93 (1989) 595-615.
- [25] O. Awad, E.L. Dedkov, C. Jiao, S. Bloomer, R.J. Tomanek, G.C. Schattman, Differential healing activities of CD34+ and CD14+ endothelial cell progenitors, *Arterioscler. Thromb. Vasc. Biol.* 26 (2006) 758-764.
- [26] T. Ziegelhoeffer, B. Fernandez, S. Kostin, M. Heil, R. Voswinckel, A. Helisch, W. Schaper, Bone marrow-derived cells do not incorporate into the adult growing vasculature, *Circ. Res.* 94 (2004) 230-238.
- [27] L. Zentilin, S. Tafuro, S. Zacchigna, N. Arsic, L. Pattarini, M. Sinigaglia, M. Giacca, Bone marrow mononuclear cells are recruited to the sites of VEGF-induced neovascularization but are not incorporated into the newly formed vessels, *Blood* 107 (2006) 3546-3554.
- [28] U.M. Gehling, S. Ergun, U. Schumacher, C. Wagener, K. Pantel, M. Otte, G. Schuch, P. Schafhausen, T. Mende, N. Kilic, K. Kluge, B. Schafer, D.K. Hossfeld, W. Fiedler, In vitro differentiation of endothelial cells from AC133-positive progenitor cells, *Blood* 95 (2000) 3106-3112.
- [29] J. Yamashita, H. Itoh, M. Hirashima, M. Ogawa, S. Nishikawa, T. Yurugi, M. Naito, K. Nakao, S. Nishikawa, Flk1-positive cells derived from embryonic stem cells serve as vascular progenitors, *Nature* 408 (2000) 92-96.
- [30] P. Romagnani, F. Annunziato, F. Liotta, E. Lazzari, B. Mazzinghi, F. Frosali, L. Cosmi, L. Maggi, L. Lasagni, A. Scheffold, M. Kruger, S. Dimmeler, F. Marra, G. Gensini, E. Maggi, S. Romagnani, CD14+CD34low cells with stem cell phenotypic and functional features are the major source of circulating endothelial progenitors, *Circ. Res.* 97 (2005) 314-322.
- [31] H. Iwaguro, J. Yamaguchi, C. Kalka, S. Murasawa, H. Masuda, S. Hayashi, M. Silver, T. Li, J.M. Isner, T. Asahara, Endothelial progenitor cell vascular endothelial growth factor gene transfer for vascular regeneration, *Circulation* 105 (2002) 732-738.
- [32] S. Murasawa, J. Llevadot, M. Silver, J.M. Isner, D.W. Losordo, T. Asahara, Constitutive human telomerase reverse transcriptase expression enhances regenerative properties of endothelial progenitor cells, *Circulation* 106 (2002) 1133-1139.
- [33] S. Fuchs, A. Motta, C. Migliaresi, C.J. Kirkpatrick, Outgrowth endothelial cells isolated and expanded from human peripheral blood progenitor cells as a potential source of autologous cells for endothelialization of silk fibroin biomaterials, *Biomaterials* 31 (2006) 5399-5408.
- [34] D. Schmidt, L.M. Asmis, B. Odermatt, J. Kelm, C. Breymann, M. Gossi, M. Genoni, G. Zund, S.P. Hoerstrup, Engineered living blood vessels: functional endothelia generated from human umbilical cord-derived progenitors, *Ann. Thorac. Surg.* 82 (2006) 1465-1471.
- [35] T. Aper, A. Schmidt, M. Duchrow, H.P. Bruch, Autologous blood vessels engineered from peripheral blood sample, *Eur. J. Vasc. Endovasc. Surg.* 33 (2006) 33-39.

Full Paper

The Novel Compounds That Activate Farnesoid X Receptor: the Diversity of Their Effects on Gene Expression

Takuo Suzuki^{1,2,*}, Norimasa Tamehiro³, Yoji Sato⁴, Tetsu Kobayashi¹, Akiko Ishii-Watabe¹, Youichi Shinozaki⁵, Tomoko Nishimaki-Mogami³, Toshihiro Hashimoto⁶, Yoshinori Asakawa⁶, Kazuhide Inoue⁷, Yasuo Ohno⁵, Teruhide Yamaguchi¹, and Toru Kawanishi¹

¹Division of Biological Chemistry and Biologicals, ³Division of Biosignaling, ⁴Division of Cellular and Gene Therapy Products, ⁵Division of Pharmacology, National Institute of Health Sciences, Tokyo 158-8501, Japan

²Pharmaceuticals and Medical Device Agency, Tokyo 100-0013, Japan

⁶Faculty of Pharmaceutical Sciences, Tokushima Bunri University, Tokushima 770-8514, Japan

⁷Graduate School of Pharmaceutical Sciences, Kyushu University, Fukuoka 812-8582, Japan

Received January 8, 2008; Accepted May 16, 2008

Abstract. Farnesoid X receptor (FXR) controls the expression of critical genes in bile acid and cholesterol homeostasis. To study FXR and to develop a regulator of cholesterol, some non-steroidal and steroidal ligands have been found in addition to endogenous ligands for FXR. In this study, we discovered five bile acid derivatives (methyl cholate, methyl deoxycholate, 5 β -cholanic acid, 5 β -cholanic acid-7 α ,12 α -diol, and NIHS700) and two natural products (marchantin A and marchantin E) that activated FXR in the reporter assay. These compounds activated FXR to a high level comparable to the most potent endogenous bile acid, chenodeoxycholic acid, although it was not predicted from their structures; five of them were similar to the lower potency bile acids, and two were structurally much different from bile acids. The elevation levels of reporter gene expression by some of the screened compounds were varied in Cos-7, HepG2, HuH-7, and Caco-2 cells. These compounds also controlled the expression of genes regulated by FXR, and some of the compounds regulated these genes in a cell-type-specific and/or gene-selective fashion. Therefore, molecular design of the compounds can cause selective modulation of the expression of FXR target genes.

Keywords: farnesoid X receptor (FXR), reporter assay, ginkgolic acid, marchantin, cell-type-specific modulation

Introduction

The farnesoid X receptor (FXR, *NR1H4*) is a member of the nuclear-receptor superfamily. Nuclear receptors are ligand-activated transcription factors that are involved in a variety of physiological, developmental, and toxicological processes. The nuclear-receptor superfamily includes receptors for thyroid and steroid hormones, retinoids, and vitamin D, as well as receptors for unknown ligands. These receptors share a highly conserved DNA-binding domain and a discrete ligand-binding domain; and they bind to hormone response

elements (HRE) on the DNA during the formation of homodimers, heterodimers, or monomers. The ligand-binding to nuclear receptors leads to a conformational change of these receptors and the recruitment of coactivator complexes, resulting in transcriptional activation (1). Their ligand-dependent activity makes nuclear receptors good pharmacological targets.

FXR is a receptor for bile acids such as chenodeoxycholic acid (CDCA), deoxycholic acid, cholic acid, and their conjugates. Bile acids are synthesized in the liver and secreted into the intestine, where their physical properties facilitate the absorption of fats and vitamins through micelle formation. Cholesterol disposal from the liver is also dependent on the bile acid composition of the secreted bile. FXR is activated by bile acids and controls the expression of critical genes in bile

*Corresponding author (affiliation #1). tsuzuki@nihs.go.jp
Published online in J-STAGE on July 5, 2008 (in advance)
doi: 10.1254/jphs.08006FP

acid and cholesterol homeostasis such as the bile salt export pump (*BSEP*), small heterodimer partner (*SHP*), *CYP7A1*, ileal bile acid-binding protein (*IBABP*), and phospholipid transfer protein (*PLTP*) (2–4). FXR plays a critical role in lipid metabolism since FXR-null mice showed elevated serum cholesterol and triglyceride levels (5), and an FXR agonist has been shown to reduce serum triglyceride levels (6). Moreover, an FXR agonist has been reported to confer hepato-protection in a rat model of cholestasis (7). Recently, FXR has also been reported to mediate glucose metabolism and to protect the intestinal mucosa from bacterial overgrowth and inflammatory insults (8, 9). Therefore, the development of FXR agonists might prove useful for the treatment of a wide variety of diseases, including diabetes, cholesterol gallstones, and hepatic and intestinal toxicity.

In addition to bile acids, some compounds whose structures are much different from bile acids (e.g., GW4064) and several selective modulators (e.g., guggulsterone and AGN34) that regulate a subset of FXR-specific genes have been identified as FXR ligands (10, 11). These compounds other than bile acids are useful for analysis of the role of FXR in lipid and glucose metabolism because they may not have the FXR-independent property of bile acids (e.g., dietary lipid absorption) and are not metabolized to form harmful lithocholic acid. On the other hand, selective ligands have been studied in detail regarding the other nuclear receptors (e.g., selective estrogen-receptor modulators (SERMs)). These compounds exhibit variable effects (e.g., function as agonists or antagonists) depending on the cells and tissues, and they have been used in therapy (e.g., tamoxifen and raloxifen). Because FXR has been found to play many roles in addition to lipid metabolism, selective FXR modulators might be useful for therapy.

We previously reported the reporter assay system of FXR, RAR, and RXR using green fluorescent protein derivatives (12). We screened a compound library (NIHS library containing about 700 compounds) and found five bile acid derivatives (methyl cholate, methyl deoxycholate, 5 β -cholic acid, 5 β -cholic acid-7 α ,12 α -diol, and NIHS700) and two natural products (marchantin A and marchantin E) as FXR activators. Concerning these seven compounds and ginkgolic acids that we previously showed as FXR activators, we investigated the FXR activation by reporter assay in four types of cells and the expression of the genes regulated by FXR. These compounds activated FXR comparably to the most potent bile acid, and some controlled the expression of genes regulated by FXR in a cell-type-specific and/or gene-selective fashion.

Materials and Methods

Chemicals

Methyl cholate, methyl deoxycholate, 5 β -cholic acid, and 5 β -cholic acid-7 α ,12 α -diol were purchased from Steraloids, Inc. (Newport, RI, USA). NIHS700 was provided from Research Foundation Itsuu Laboratory (Tokyo). Ginkgolic acid 15:1 was purified *Ginkgo biloba* L. var. *diptera* as described previously (12). Ginkgolic acid 17:1 was purchased from Nagara Science (Gifu). Chenodeoxycholic acid was purchased from Sigma-Aldrich (St. Louis, MO, USA). Cholic acid, deoxycholic acid and lithocholic acid were purchased from Wako (Osaka).

Isolation of marchantins A and E from *Marchantia paleacea* var. *diptera*

Fresh material (6.67 kg) of *Marchantia paleacea* var. *diptera* collected in Tokushima, Japan in 1993 was extracted with MeOH (10 L) for 1 month at room temperature. The extract was filtered and evaporated *in vacuo* to afford a brown residue (176.0 g), which was subjected repeatedly to column chromatography (CC) on silica gel (*n*-hexane-EtOAc, gradient) and Sephadex-LH-20 (CHCl₃-MeOH = 1:1) to afford marchantin A (79.5 g) and marchantin E (8.34 g) (13, 14).

Plasmid construction

The construction of plasmids for the reporter assay using green fluorescent protein (GFP) derivatives has been described in a previous report (12). For expression of FXR and RXR α , the ORF region of human FXR or human RXR α (accession number U68233, X52773) was inserted into pcDNA3.1 (Invitrogen, Carlsbad, CA, USA). For reporter plasmids, the FXR response element (4 copies of DR1: ggatccaaactgaGGGTCAGTGACCC aagtgaaaaactgaGGGTCAGTGACCCcaagtgaattcaact gagGGTCAGTGACCCcaagtgaaaaactgaGGGTCAGTGACCCcaagtgaatct), the 3' region (201 bp) of cytomegalovirus (CMV201) promoter, and enhanced yellow fluorescent protein (EYFP) were ligated. As an internal control plasmid, the luciferase gene of pGL3-Control Vector (Promega, Madison, WI, USA) was replaced with enhanced cyan fluorescent protein (ECFP).

For a reporter assay using luciferase, FXRE was inserted into the *Mlu*I and *Bgl*II sites of pGL3-Control Vector, and the SV40 promoter was replaced with minimal CMV promoter. The pRL-CMV vector (Promega) was used as an internal control vector.

The reporter assay using GFP derivatives

A monkey kidney cell line, COS-7, was kept in DMEM (Sigma-Aldrich) with penicillin (100 unit/ml),

streptomycin (100 µg/ml), and 10% FBS. Transfections were performed using Effectene transfection reagent (Qiagen, Valencia, CA, USA) according to the manufacturer's instructions. The ratio of the reporter plasmid, FXR expression plasmid, RXR expression plasmid, and the internal control plasmid was 4:1:1:1. The culture medium was replaced with DMEM without phenol red (GIBCO, Carlsbad, CA, USA) supplemented with 10% charcoal-treated FBS (Hyclone, Logan, UT, USA) when the transfections were performed. At 15 h after transfection, the cells were treated with trypsin-EDTA (GIBCO) and divided among wells of a black 96-well plate with 100 µl of the culture medium. At 6 h after division among wells, the cells were treated with chemicals. After 40-h incubation, the medium was eliminated by decantation, the cells were washed twice with PBS, and the wells were filled with 200 µl PBS. Fluorescence was detected using a microplate reader (ARVO; Perkin Elmer, Fremont, CA, USA). The fluorescence of EYFP was detected with an excitation filter of 485 nm and an emission filter of 545 nm, and that of ECFP was detected with filters of 420 nm and 486 nm (Perkin Elmer), respectively. The autofluorescence in COS-7 cells was subtracted from each of the detected fluorescences, and the EYFP/ECFP ratio was calculated using the resulting values.

The reporter assay using luciferase

The human hepatocyte cell line HepG2 was kept in MEM (Sigma-Aldrich) with penicillin (100 unit/ml), streptomycin (100 µg/ml), and 10% FBS. The cells were transfected with 3 times more plasmids than recommended with salmon sperm DNA (200 ng for 1 well of a 6-well plate) using Effectene transfection reagent (Qiagen). In contrast, the human hepatocyte cell line HuH-7 was kept in DMEM with penicillin (100 unit/ml), streptomycin (100 µg/ml), and 10% FBS; and the human intestinal cell line Caco-2 was kept in DMEM with penicillin (100 unit/ml), streptomycin (100 µg/ml), 10% FBS, and 100 µM MEM Non-Essential Amino Acids Solution (GIBCO). HuH-7 and Caco-2 cells were transfected with plasmids using Effectene transfection reagent (Qiagen) according to the manufacturer's instructions. The ratio of the reporter plasmid using luciferase, the FXR expression plasmid, RXR expression plasmid, and the internal control plasmid using *renilla* luciferase was 4:1:1:1. FBS of the culture medium was replaced with charcoal-treated FBS (Hyclone) when the transfections were performed. The following manipulations were the same as those used in the reporter assay with GFP derivatives. After 40-h treatment with the compounds, measurement of luciferase and *renilla* luciferase was performed with

the Dual-Glo™ Luciferase Assay System (Promega) according to the manufacturer's instructions.

TaqMan primers and probes

Oligonucleotide primers and probes for human *BSEP*, *SHP*, and *CYP7A1* were synthesized by Applied Biosystems (Foster City, CA, USA). These sequences (5' to 3') were as follows: Human *BSEP*, forward primer (GGCCATGTACGAGATCCTAA), probe (6FAM-TCTTGCTACTAGATGAAGCCACTTCTGCCTTAGA-TAMRA) and reverse primer (TGCACCGTCTTT CACTTTCTG); Human *SHP*, forward primer (GGTG CAGTGGCTTCAATGC), probe (6FAM-TCTGGAG CCTGGAGCTTAGCCCCA-TAMRA), and reverse primer (GGTTGAAGAGGATGGTCCCTTT); Human *CYP7A1*, forward primer (GAGAAGGCAAACGGGT-GAAC), probe (6FAM-TGGATTAATCCATACCTG GGCTGTGCTCT-TAMRA), and reverse primer (GGT ATGACAAGGGATTTGTGATGA). The primers and probe for 18S rRNA were also purchased from Applied Biosystems.

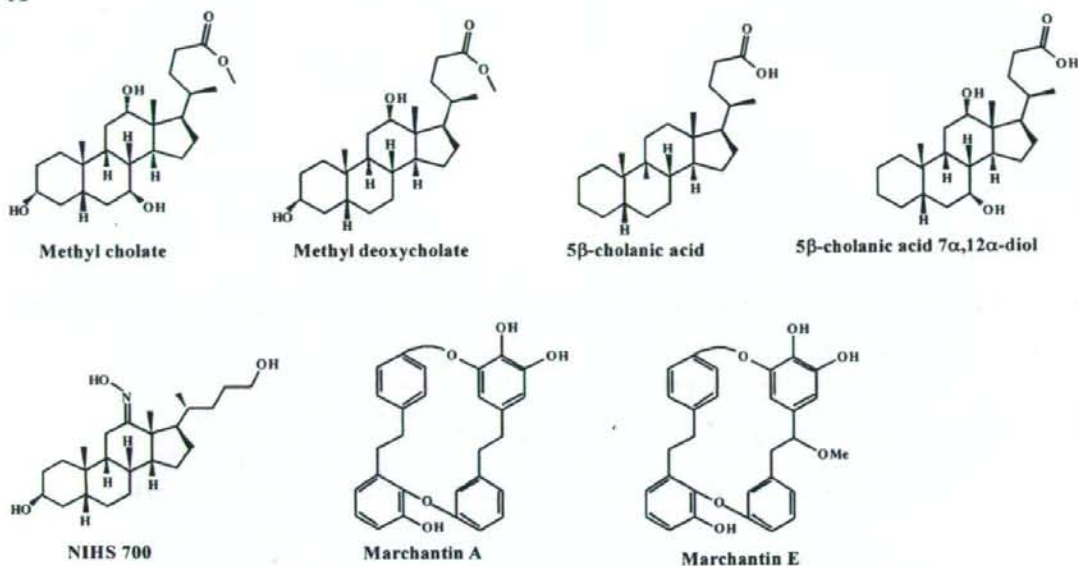
RNA isolation and real-time quantitative PCR

The culture medium of HepG2, HuH-7, and Caco-2 cells was replaced with the medium supplemented with 10% charcoal-treated FBS (Hyclone) at 24 h before treatment with the compounds. The cells were treated with the tested chemicals for 24 h, and total RNA was then prepared using the RNeasy purification system according to the manufacturer's instructions (Qiagen). Reverse transcription reactions and TaqMan-PCRs were performed using the High-Capacity cDNA Archive Kit (Applied Biosystems) and the TaqMan Universal PCR Master Mix (Applied Biosystems) according to the manufacturer's instructions. Sequence-specific amplification was quantified with the ABI Prism 7700 sequence detection system (Applied Biosystems), and values were normalized to 18S rRNA.

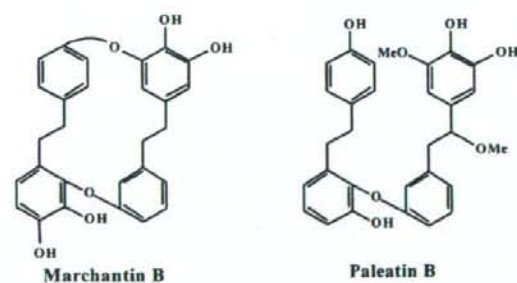
Results

We found seven compounds that activate FXR (the chemical structures of which are shown in Fig. 1A) using the reporter assay system described by Suzuki et al. (12). In the reporter assay system, two fluorescent proteins, EYFP and ECFP, were used for detection of FXR activation and as an internal control, respectively. The activation of FXR by the seven compounds and some endogenous ligands [i.e., cholic acid (CA), deoxycholic acid (DCA), lithocholic acid (LCA), and chenodeoxycholic acid (CDCA)] is shown as the increased ratio of EYFP/ECFP fluorescence intensity in the upper panel of Fig. 2A. As a control, the reporter vector

A



B



C

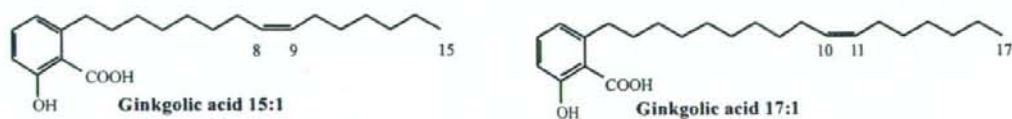


Fig. 1. Structure of the compounds that activated FXR and their related compounds. A: Structure of the compounds that activated FXR as determined by the reporter assay. B: The compounds similar to marchantin A and marchantin E. C: Ginkgolic acid 15:1 and ginkgolic acid 17:1 that highly activated FXR described in Ref. 12.

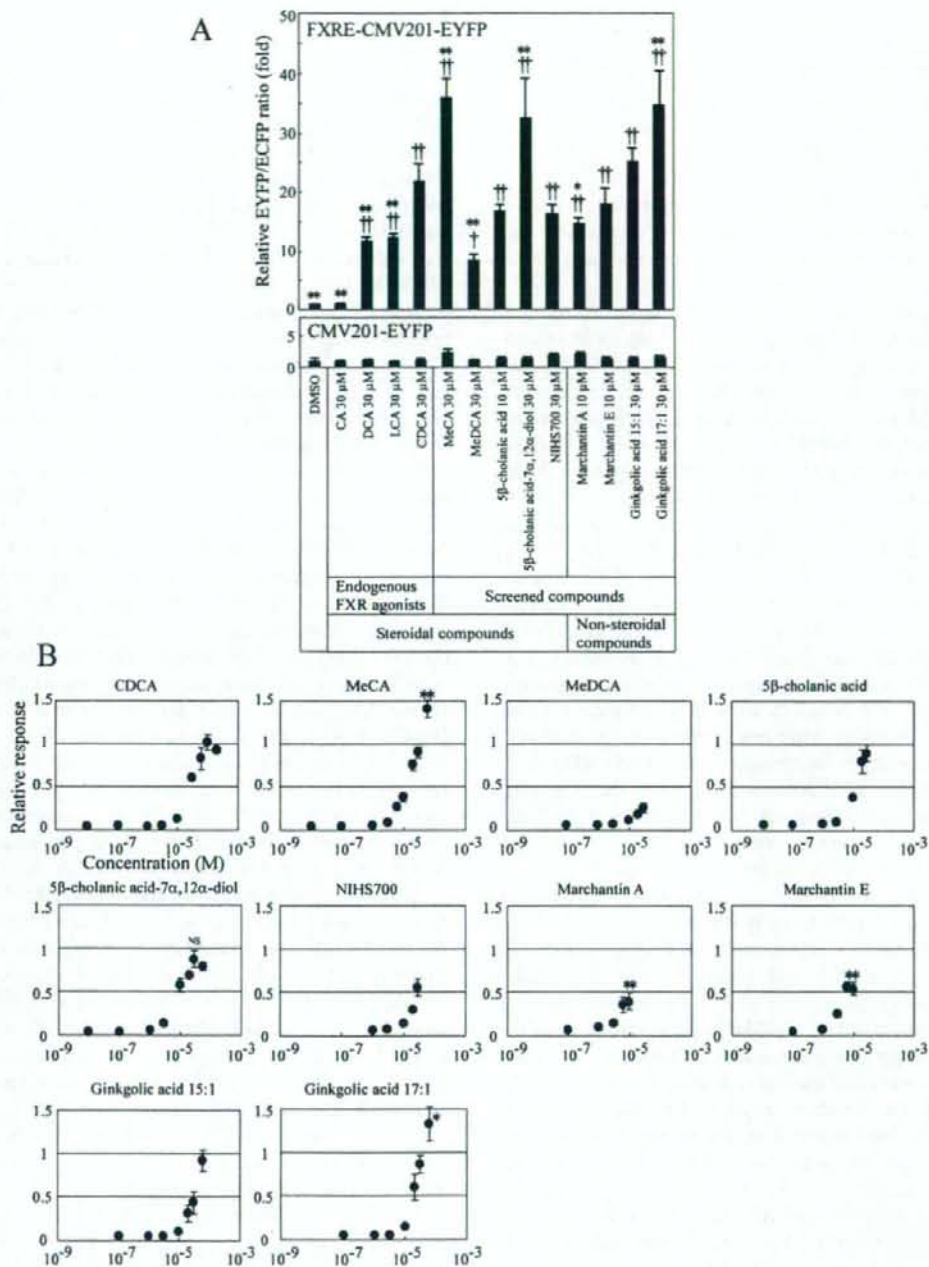


Fig. 2. Response in the reporter expression. **A:** The activation of FXR. COS-7 cells were transfected with the reporter plasmid containing FXRE, the expression plasmids of FXR and RXR α , and the internal control plasmid. The transfected cells were treated with each compound. All values are means \pm S.D., $n = 4$. $^{\dagger}P < 0.05$ vs DMSO, $^{\ddagger}P < 0.01$ vs DMSO, $^*P < 0.05$ vs CDCA (30 μ M), $^{**}P < 0.01$ vs CDCA (30 μ M), according to Dunnett's test. **B:** Dose-response analyses on the reporter assay of FXR. The response was shown as a ratio, compared with that by CDCA at 100 μ M. All values are means \pm S.D., $n = 4$. $^*P < 0.05$, $^{**}P < 0.01$; NS, not a significant difference, compared with CDCA at 100 μ M according to Student's t -test.

without FXR response element was used in place of the reporter vector to determine the response by the unexpected factors (the change in the transcriptional efficiency unrelated to FXR, the self-fluorescence of the tested chemicals, and so forth) (lower panel of Fig. 2A). Moreover, it was confirmed that these seven compounds activated the expression of the reporter gene EYFP via FXR because the induction of EYFP expression required cotransfection of an FXR expression vector and the compounds did not activate RXR homodimer and RAR-RXR heterodimer (data not shown).

The seven compounds could be separated into 2 groups: those that contained steroid skeletons and those that did not (Fig. 1A). The compounds in the former group were methyl cholate (MeCA), methyl deoxycholate (MeDCA), 5 β -cholic acid, 5 β -cholic acid-7 α ,12 α -diol, and NIHS700. Methyl cholate and methyl deoxycholate are methyl esters of endogenous FXR ligands (i.e., cholic acid and deoxycholic acid). FXR was also activated by 5 β -cholic acid and 5 β -cholic acid-7 α ,12 α -diol, whose structures differed only in the 3 α -hydroxyl group from endogenous FXR ligands (i.e., lithocholic acid and cholic acid). The structure of NIHS700 was different from that of lithocholic acid at the substituents of the 11- and 24-positions. The compounds in the latter group, non-steroidal compounds, were marchantin A and marchantin E that were isolated from the liverwort *Marchantia* species (13). Although these two compounds strongly activated FXR (Fig. 2A), marchantin B and paleatin B (shown in Fig. 1B), analogues of marchantin A and marchantin E, did not cause such activation, even at higher concentrations (data not shown). The difference between marchantin A and marchantin B is only one hydroxyl group, and that between marchantin E and paleatin B is ring-opening or not. Along with the seven compounds shown in Fig. 1A, ginkgolic acid 15:1 and ginkgolic acid 17:1 (their structures are shown in Fig. 1C and the activation of FXR is shown in Fig. 2A), the major constituents of the crude extracts from ginkgo leaves that highly activated FXR (12) were also studied in detail in the present study.

In Fig. 2B, we show the dose-dependency of these compounds as compared to the maximal response by the most potent endogenous ligand, CDCA. All the compounds were hydrophobic and could not be dissolved at over 30–60 μ M, each, in culture medium. Moreover, responses by some compounds even at soluble concentrations (Marchantin E at 30 μ M and MeDCA at 60 μ M) could not be measured due to their toxicity. Therefore, we could not obtain the data at higher concentrations. Although the value of treatment with 30 μ M 5 β -cholic acid is shown in Fig. 2B, this compound slightly separated out from the solution at

this concentration. Therefore, the concentration applied in the other experiments was limited to 10 μ M. Since the EC₅₀ values of 5 β -cholic acid-7 α ,12 α -diol, marchantin A, and marchantin E could be estimated to be 3–10, 3–6, and 3–6 μ M, respectively, the values were lower than that of CDCA (approximately 30 μ M). Maximal activation by 5 β -cholic acid-7 α ,12 α -diol was comparable to that by CDCA, but those by the marchantins were lower ($P < 0.01$). The EC₅₀ and maximal values of MeCA, MeDCA, 5 β -cholic acid, NIHS700, and ginkgolic acids could not be assessed because of low solubility or toxicity. However, activations of FXR by 60 μ M of MeCA and ginkgolic acid 17:1 were higher than maximal activation by CDCA. Since the EC₅₀ values of the 6 compounds could not be estimated, we analyzed activations by all the compounds at 30 or 10 μ M in the following experiments.

Since FXR was primarily localized in the liver and intestine, we determined that the compounds also act as FXR activators in cultured hepatoma and intestinal cancer cells (HepG2, HuH-7, and Caco-2 cells). The reporter assay using GFP derivatives could be applied to these cell lines. However, the signal of the internal control was less than in COS-7 cells because the internal control plasmid was not replicated in the cells without large T antigen. We therefore used luciferase (LUC) and *renilla* luciferase (RLUC) for the reporter assay in HepG2, HuH-7, and Caco-2 cells. The extent of the induction with some compounds differed among the cells on the basis of the activation extent by endogenous ligands (Figs. 2A and 3). The differences are enumerated below. Reporter expression was strongly induced by MeCA to higher level than by CDCA in COS-7, moderately induced in HuH-7, and only weakly induced to a lower level than by CDCA in HepG2. Marchantins (A and E) scarcely induced the expression in HepG2. MeDCA induced the expression higher than LCA in HepG2 ($P < 0.05$, according to Student's *t*-test), but lower than LCA in COS-7 ($P < 0.01$). The induction by ginkgolic acid 17:1 in HepG2 was lower than that by CDCA, but higher in COS-7. Moreover, the induction by NIHS700 in Caco-2 was lower than that by LCA ($P < 0.05$, according to Student's *t*-test), but higher in COS-7 ($P < 0.01$). These compounds seemed to activate FXR in a cell-type-specific fashion.

We then examined the effects of the screened compounds on the expression of genes regulated by FXR. FXR controls the expression of critical genes in bile acid and cholesterol homeostasis (2–4). In this experiment, we detected the expression of three genes, bile salt export pump (*BSEP*), small heterodimer partner (*SHP*), and *CYP7A1*. By FXR activation, the expression of *BSEP* and *SHP* genes are directly upregulated, and

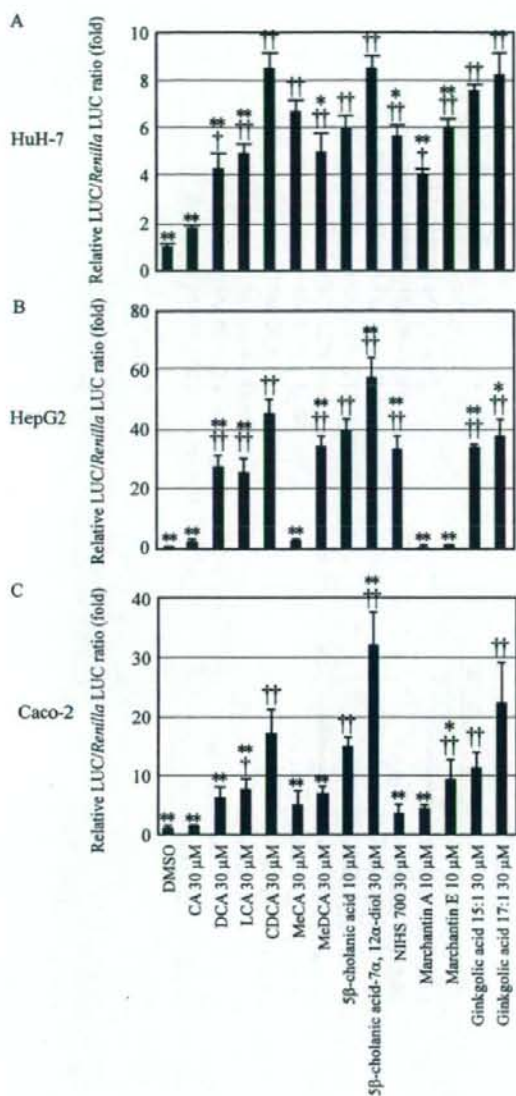


Fig. 3. The difference of FXR-activation in the reporter assay. A: The activation of FXR in HuH-7 cells is shown. HuH-7 cells were transfected with the reporter plasmid containing FXRE and luciferase, the expression plasmids of FXR and RXR α , and the internal control plasmid containing *renilla* luciferase. The transfected cells were treated with each compound. Data are shown as the means \pm S.D. derived from four wells. $^{\dagger}P < 0.05$ vs DMSO, $^{\ddagger}P < 0.01$ vs DMSO, $^*P < 0.05$ vs CDCA (30 μ M), $^{**}P < 0.01$ vs CDCA (30 μ M), according to Dunnett's test. The activation of FXR in HepG2 and Caco-2 cells is shown in the middle and lower panel, respectively. Except for the cell type, all manipulations were the same as those shown above. B: HepG2 cells, $n = 4$. C: Caco-2 cells, $n = 4 - 5$.

that of *CYP7A1* gene is indirectly down-regulated. HepG2 cells without transfection of artificial genes were treated with the compounds, and the amount of the mRNAs was measured by real-time quantitative PCR. The expression of the genes in HepG2 cells is shown in Fig. 4 (A - C). The compounds other than MeCA, 5 β -cholanic acid, marchantin A, and marchantin E significantly induced the expression of *SHP* mRNA ($P < 0.05$ vs DMSO, according to Dunnett's test). Because *BSEP* was expressed only at low levels in HepG2 cells, Fig. 4C showed scattered results. However, the change in *BSEP* expression was similar to the change in *SHP* expression. On the other hand, the reduction levels of *CYP7A1* mRNA by some compounds differed from the change of *SHP* mRNA levels. The reduction in *CYP7A1* mRNA accumulation by MeDCA was lower than that by CDCA, although the compound induced *SHP* mRNA accumulation to a higher level than CDCA. Moreover, marchantin A and E reduced *CYP7A1* mRNA accumulation ($P < 0.05$ vs DMSO), although the regulation of *SHP* mRNA accumulation was not detected.

Moreover, regulation of gene expression in a cell-type-specific fashion was also detected (Fig. 4D). The induction of *BSEP* expression by MeCA in HuH-7 cells was higher than that of *BSEP* and *SHP* expression in HepG2 cells, and that by MeDCA was lower. These results indicate that the screened compounds could regulate the expression of critical genes in bile acid and cholesterol homeostasis and suggested that MeCA, MeDCA, marchantin A, and marchantin E possibly regulate expression of the genes in a cell-type-specific and/or gene-species selective fashion.

Discussion

In this paper, we found five steroidal compounds and two non-steroidal compounds that activate FXR. These compounds possess some properties that differ from those of CDCA.

First, two of the steroidal compounds, 5 β -cholanic acid and 5 β -cholanic acid-7 α ,12 α -diol, were found to be effective ligands for FXR in a reporter assay and in quantitative real-time PCR. The crystal structure of the FXR ligand binding domain was analyzed as a complex with 3-deoxyCDCA and revealed that the 3-hydroxyl group was not responsible for the activation of FXR (15). However, FXR was activated to lower levels by lithocholic acid and cholic acid, whose structures were different only in the 3 α -hydroxyl group from 5 β -cholanic acid and 5 β -cholanic acid-7 α ,12 α -diol. In this case, elimination of the 3-hydroxyl group increased the potency of the activation.

The other three steroidal compounds were MeCA,

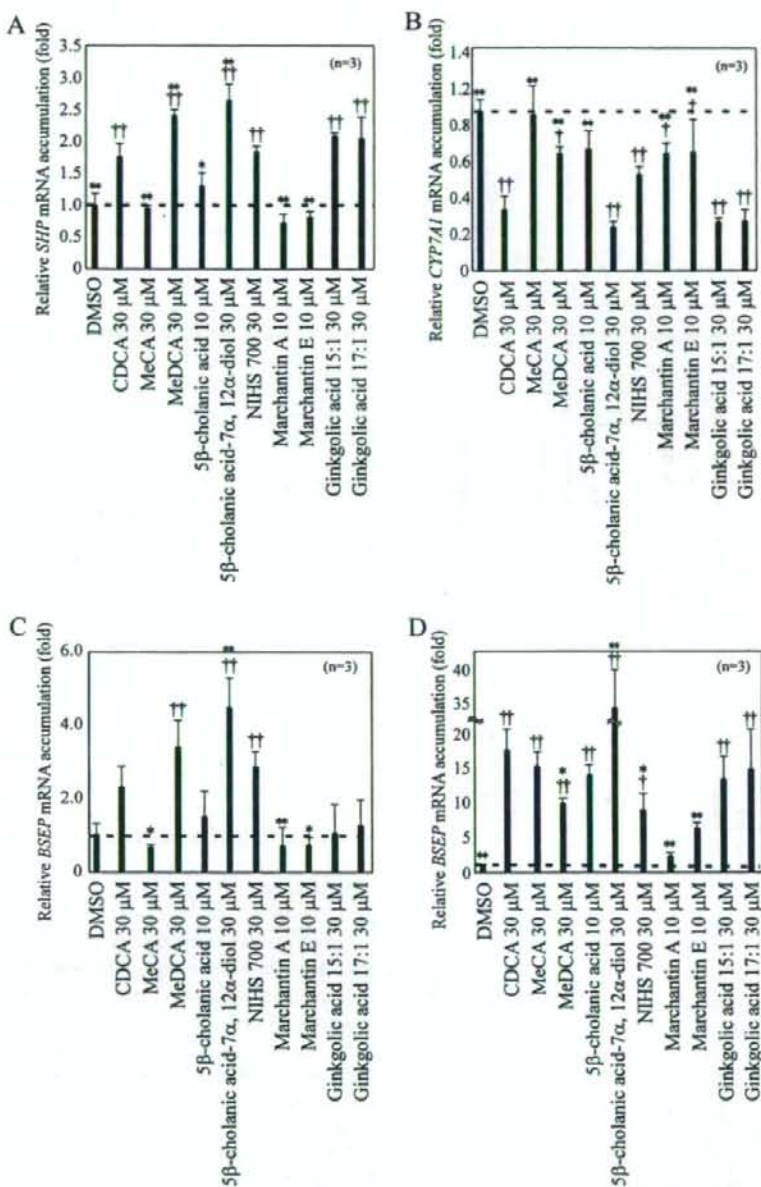


Fig. 4. Expression of *SHP*, *CYP7A1*, and *BSEP* genes in cells treated with the compounds. HepG2 cells were treated with each compound for 24 h. Accumulation of *SHP* (A), *CYP7A1* (B), and *BSEP* (C) mRNA in HepG2 cells was detected by real-time quantitative PCR. D: Accumulation of *BSEP* mRNA in HuH-7 cells treated with each compound for 24 h. All values are means \pm S.D., $n = 3$. $^{\dagger}P < 0.05$ vs DMSO, $^{\ddagger}P < 0.01$ vs DMSO, $^*P < 0.05$ vs CDCA (30 μ M), $^{**}P < 0.01$ vs CDCA (30 μ M), according to Dunnett's test.

MeDCA, and NIHS700. Although the structures of these compounds were similar to those of the endogenous

ligands, the slight modification of bile acids caused different regulation of FXR. It has been suggested that

the binding of bile acids with a slightly different structure (CA, DCA, UDCA, and CDCA) resulted in different FXR conformations, which in turn differentially regulated expression of individual FXR targets (16). Therefore, these compounds may also produce different FXR conformations than that produced by CDCA. In fact, MeDCA showed different properties in the regulation of the genes as compared to CDCA. DCA, CA, and UDCA have been reported to partially increase *BSEP* expression, but repress *CYP7A* mRNA with nearly equal effects as CDCA (16). Adversely, MeDCA strongly induced *BSEP* mRNA, but only weakly reduced *CYP7A1* mRNA (Fig. 4: B and C). It is possible that the *CYP7A1* expression was also influenced by other factors such as c-jun N-terminal kinase and xenobiotic receptor (17, 18). However, since MeDCA possibly induces the export of bile acids from hepatocytes without disturbing catabolization from cholesterol to bile acids, they might effectively improve the disorder of cholesterol and bile acids. NIH700 seemed to have properties similar to those of MeDCA, although statistically significant differences could not be observed by Dunnett's test. Therefore, further analyses about MeDCA and NIH700 are needed for effective regulation of FXR.

Since MeCA and MeDCA are methyl esters of endogenous FXR ligands, there is a question about whether these compounds are hydrolyzed and act as CA or DCA. Considering that MeDCA showed different properties in the gene expression as compared to DCA, these compounds did not seem to act as hydrolyzed forms.

The compounds screened in this study contained several non-steroidal chemicals. Marchantin A was isolated from the liverwort *Marchantia* species, as its major component (13). It shows antifungal, antimicrobial, cytotoxic, muscle-relaxing, and 5-lipoxygenase, cyclooxygenase, and calmodulin inhibitor activities [reviewed in by Asakawa et al. (19)]. The compounds with a slight structural change from marchantin A and E (i.e., marchantin B and paleatin B) did not activate FXR. It may be interesting to examine the mechanism of binding to FXR and that of the subsequent regulation of the target genes. Since these two compounds and ginkgolic acids have a much different structure from bile acids, the structural change of FXR in response to these compounds might be different from that in response to bile acids, which might result in different regulation pattern of the genes of bile acid homeostasis. In fact, marchantin A and marchantin E activated FXR diversely in each cell, although ginkgolic acids did not show FXR activation in a cell-type specific or gene-selective fashion. Bile acids function in the dietary lipid absorption and were reported to activate mitogen-activated protein kinase

pathways without FXR (17, 20). The non-steroidal compounds were thought not to have these functions, although it has not been clear whether these compounds have effects other than FXR activation. Moreover, the non-steroidal compounds are not metabolized to form harmful lithocholic acid (21, 22). Therefore, it is possible that these compounds can be used for studying the pharmacology of FXR.

As described above, some compounds demonstrated properties of cell-type-specific and/or gene-selective modulators. Until now, several compounds have been found to be cell-type-specific and/or gene-selective modulators of FXR (10, 11, 16). Although the mechanism of selective FXR modulation remains to be elucidated, it was suggested that differences in coregulator recruitment play a critical role in cell-type-specific and promoter-specific regulation by other nuclear receptors (23, 24). We therefore investigated the binding capacity of FXR with receptor-interacting domains of the activator for thyroid hormone and retinoid receptors (ACTR), vitamin D-interacting protein 205 (DRIP205), glucocorticoid receptor-interacting protein (GRIP), receptor-interacting protein 140 (RIP140), and steroid receptor coactivator-1 (SRC-1) with a mammalian two-hybrid assay. However, we could not detect enough obvious differences to explain the cell-type (and/or gene) specific modulation (data not shown).

There are the other possibilities about cell-type-specific modulation, although the gene specific modulation could not be explained. First, the compounds are metabolized in cultured cells and their metabolites bind to FXR as ligands. In case that the metabolism varies with cell-type, FXR is differentially-activated. Second, the compounds are inactivated by metabolism in some cells. Third, permeability of the compounds is different according to cell-type. Since all the compounds tested were hydrophobic and separated out in culture medium at lower concentrations as compared to CDCA, the third possibility is unlikely. To reveal the mechanism of selective FXR modulation and to produce a synthetic selective modulator, farther analyses are required.

Finally, FXR has pleiotropic therapeutic potential, but a simple FXR agonist will have undesired side-effects (reviewed in refs. 25 and 26). The compounds discussed in the present paper appear to be useful for studying FXR modulation leading to selective FXR modulation for therapy.

Acknowledgments

This work was supported by a grant-in-aid (MF-16) from the Pharmaceuticals and Medical Device Agency, a

grant-in-aid for Research on Publicly Essential Drugs and Medical Devices from the Japan Health Science Foundation, and a grant-in-aid from the Ministry of Health, Labour, and Welfare of Japan.

References

- Khorasanizadeh S, Rastinejad F. Nuclear-receptor interactions on DNA-response elements. *Trends Biochem Sci.* 2001;26:384-390.
- Makishima M, Okamoto AY, Repa JJ, Tu H, Learned RM, Luk A, et al. Identification of a nuclear receptor for bile acids. *Science.* 1999;284:1362-1365.
- Parks DJ, Blanchard SG, Bledsoe RK, Chandra G, Consler TG, Kliewer SA, et al. Bile acids: natural ligands for an orphan nuclear receptor. *Science.* 1999;284:1365-1368.
- Wang H, Chen J, Hollister K, Sowers LC, Forman BM. Endogenous bile acids are ligands for the nuclear receptor FXR/BAR. *Mol Cell.* 1999;3:543-553.
- Sinal CJ, Tohkin M, Miyata M, Ward JM, Lambert G, Gonzalez FJ. Targeted disruption of the nuclear receptor FXR/BAR impairs bile acid and lipid homeostasis. *Cell.* 2000;102:731-744.
- Maloney PR, Parks DJ, Haffner CD, Fivush AM, Chandra G, Plunket KD, et al. Identification of a chemical tool for the orphan nuclear receptor FXR. *J Med Chem.* 2000;43:2971-2974.
- Liu Y, Binz J, Numerick MJ, Dennis S, Luo G, Desai B, et al. Hepatoprotection by the farnesoid X receptor agonist GW4064 in rat models of intra- and extrahepatic cholestasis. *J Clin Invest.* 2003;112:1678-1687.
- Zhang Y, Lee FY, Barrera G, Lee H, Vales C, Gonzalez FJ, et al. Action of the nuclear receptor FXR improves hyperglycemia and hyperlipidemia in diabetic mice. *Proc Natl Acad Sci U S A.* 2006;103:1006-1011.
- Inagaki T, Moschetta A, Lee Y-K, Peng L, Zhao G, Downes M, et al. Regulation of antibacterial defense in the small intestine by the nuclear bile acid receptor. *Proc Natl Acad Sci U S A.* 2006;103:3920-3925.
- Cui J, Huang L, Zhao A, Lew J-L, Yu J, Sahoo S, et al. Guggulsterone is a farnesoid X receptor antagonist in coactivator association assays but acts to enhance transcription of bile salt export pump. *J Biol Chem.* 2003;278:10214-10220.
- Dussault I, Beard R, Lin M, Hollister K, Chen J, Xiao JH, et al. Identification of gene-selective modulators of the bile acid receptor FXR. *J Biol Chem.* 2003;278:7027-7033.
- Suzuki T, Nishimaki-Mogami T, Kawai H, Kobayashi T, Shinozaki Y, Sato Y, et al. Screening of novel nuclear receptor agonists by a convenient reporter gene assay system using green fluorescent protein derivatives. *Phytomedicine.* 2006;13:401-411.
- Asakawa Y. Chemical constituents of hepaticae. In: Herz W, Grisebach H, Kirby WG, editors. *Progress in the chemistry of organic natural products*, Vol. 42, Wien: Springer; 1982, p. 1-285.
- Asakawa Y. Biologically active terpenoids and aromatic compounds from liverworts and inedible mushroom *Cryptoporus volvatus*. In: Colegate SM, Molyneux RJ, editors. *Bioactive natural products: detection, isolation, and structural determination*. Florida: CRC Press; 1993, p. 319-347.
- Mi L-Z, Devarakonda S, Harp JM, Han Q, Pellicciari R, Willson TM, et al. Structural basis for bile acid binding and activation of the nuclear receptor FXR. *Mol Cell.* 2003;11:1093-1100.
- Lew JL, Zhao A, Yu J, De Pedro N, Peláez F, Wright SD, et al. The farnesoid X receptor controls gene expression in a ligand- and promoter-selective fashion. *J Biol Chem.* 2004;279:8856-8861.
- Gupta S, Stravitz RT, Dent P, Hylemon PB. Down-regulation of cholesterol 7 α -hydroxylase (*CYP7A1*) gene expression by bile acids in primary rat hepatocytes is mediated by the c-Jun N-terminal kinase pathway. *J Biol Chem.* 2001;276:15816-15822.
- Staudinger JL, Goodwin B, Jones SA, Hawkins-Brown D, MacKenzie KI, LaTour A, et al. The nuclear receptor PXR is a lithocholic acid sensor that protects against liver toxicity. *Proc Natl Acad Sci U S A.* 2001;98:3369-3374.
- Asakawa Y. Recent advances in phytochemistry of bryophytes-acetogenins, terpenoids and bis(bibenzyl)s from selected Japanese, Taiwanese, New Zealand, Argentinean and European liverworts. *Phytochemistry.* 2001;56:297-312.
- Qiao L, Han SL, Fang Y, Park JS, Gupta S, Gilfor D, et al. Bile acid regulation of C/EBP β , CREB, and c-Jun function, via the extracellular signal-regulated kinase and c-Jun NH $_2$ -terminal kinase pathways, modulates the apoptotic response of hepatocytes. *Mol Cell Biol.* 2003;23:3052-3066.
- Fischer S, Beuers U, Spengler U, Zwiebel FM, Koebe HG. Hepatic levels of bile acids in end-stage chronic cholestatic liver disease. *Clin Chim Acta.* 1996;251:173-186.
- Javitt NB. Cholestasis in rats induced by tauroolithocholate. *Nature.* 1966;210:1262-1263.
- Kodera Y, Takeyama K, Murayama A, Suzuwa M, Masuhiro Y, Kato S. Ligand type-specific interactions of peroxisome proliferator-activated receptor gamma with transcriptional coactivators. *J Biol Chem.* 2000;275:33201-33204.
- Shang Y, Brown M. Molecular determinants for the tissue specificity of SERMs. *Science.* 2002;295:2465-2468.
- Modica S, Moschetta A. Nuclear bile acid receptor FXR as pharmacological target: are we there yet? *FEBS Lett.* 2006;580:5492-5499.
- Cariou B, Staels B. FXR: A promising target for the metabolic syndrome? *Trends Pharmacol Sci.* 2007;28:236-243.

Glass-State Amorphous Salt Solids Formed by Freeze-Drying of Amines and Hydroxy Carboxylic Acids: Effect of Hydrogen-Bonding and Electrostatic Interactions

Saori KADOYA,^a Ken-ichi IZUTSU,^{*b} Etsuo YONEMOCHI,^a Katsuhide TERADA,^a Chikako YOMOTA,^b and Toru KAWANISHI^b

^a Faculty of Pharmaceutical Sciences, Toho University; 2-2-1 Miyama, Funabashi, Chiba 274-8510, Japan; and

^b National Institute of Health Sciences; 1-18-1 Kamiyoga, Setagaya, Tokyo 158-8501, Japan.

Received February 6, 2008; accepted April 4, 2008; published online April 7, 2008

We studied effect of molecular interactions on the physical properties of binary freeze-dried solids and frozen aqueous solutions using model chemicals containing various functional groups (amino, carboxyl, hydroxyl). Thermal analysis of frozen solutions containing alkyl diamines and hydroxy di- or tricarboxylic acids showed thermal transitions (T_g' : glass transition of maximally freeze-concentrated phase) at temperatures higher than those of the individual solutes. A binary frozen solution containing 80 mM 1,3-diamino-2-hydroxypropane (single-solute $T_g' < -60$ °C) and 120 mM citric acid (single-solute $T_g' = -55.0$ °C) made the transition at -30.8 °C. The molecular weight of the solutes had smaller effects on the transition temperatures of the frozen mixture component solutions. Lyophilization of some high T_g' mixture frozen solutions (e.g., 1,3-diamino-2-hydroxypropane and citric acid) resulted in cake-structure amorphous solids with glass transition temperatures (T_g) higher than those of the individual components. Networking of intense hydrogen-bondings and electrostatic interactions between the heterogeneous molecules through the multiple functional groups was suggested to reduce the component mobility in the amorphous freeze-concentrated phase and the freeze-dried solids. Controlling the interactions should be a key to optimizing the physical properties of multi-component amorphous freeze-dried pharmaceutical formulations.

Key words freeze-drying; glass solid; thermal analysis; molecular interaction; salt

Glass-state amorphous solids are applied to pharmaceutical formulations as a way to improve dissolution of hydrophobic active ingredients (APIs) or to ensure stability of embedded biomacromolecules (e.g., recombinant proteins) and drug delivery system (DDS) carriers (e.g., liposome).^{1–3} Freeze-drying is often a preferable method over other procedures (e.g., quench-cooling of heat-melt solids) for the large-scale production of glass-state solid formulations containing thermally unstable ingredients. Dispersion of drug molecules into nonionic excipient matrices (e.g., trehalose, polyvinylpyrrolidone (PVP)) is a popular way to make the non-crystalline formulations of many APIs that have intrinsic propensity for crystallization or low glass transition temperatures (T_g).¹ Insufficient miscibility with certain drug molecules and poor storage stability, however, often hinders the development of solid dispersion formulations using the non-ionic matrices.

The application of salts or binary complexes is another approach to obtain stable amorphous solids.⁴ For example, freeze-drying of sodium indomethacin results in an amorphous solid that has a glass transition temperature (120 °C) significantly higher than that of the free acid molecules (45 °C).^{4,5} Recent studies indicated that the glass-state solids composed of excipient salts or salt-forming excipient combinations are promising as dispersion matrices.^{6,7} Some pH-adjusting buffer salts (e.g., monosodium citrate) form high T_g amorphous solids applicable to protein formulations.⁷ Co-lyophilization of some basic amino acids (e.g., L-arginine, L-lysine, L-histidine) with multivalent inorganic acids (e.g., phosphoric acid) also results in the formation of protein-stabilizing glass-state solids.⁶ High transition temperatures of the mixture freeze-dried solids suggest the contribution of

strong intermolecular or inter-ion interactions to reducing the heterogeneous component mobility.

In contrast to the extensive studies on the physical properties and local structure of amorphous glass- or rubber-state solids composed of nonionic small molecules (e.g., sucrose, sorbitol) or polymers (e.g., PVP),³ mechanisms that determine character of organic salts and/or heterogeneous components have not been well elucidated.^{1,3} Recent intensive studies on ionic liquids (RTMS: room temperature molten salts) provided valuable information regarding the component ion structures, participating interactions, and the physical properties of the microscopically unordered non-crystalline salt systems.⁸ Some earlier studies indicated feasibility to control the physical property of the amorphous salt solids by optimizing the component structure (e.g., ion radius in indomethacin alkali metal salts)⁴ and their compositions that determine the intermolecular and/or inter-ion interactions.

The purpose of this study was to elucidate the contribution of functional groups and the size of consisting molecules to the physical properties of multi-component frozen aqueous solutions and their freeze-dried solids. Thermal analysis of various combinations of model chemicals containing amino, carboxyl, and/or hydroxyl groups was performed to obtain the thermal transition temperatures (T_g , T_g' : glass transition temperature of maximally freeze-concentrated phase) and propensity for crystallization in the frozen solutions and freeze-dried solids. Mid- and near-infrared analysis was performed to elucidate the molecular interaction in the freeze-dried solids. We also discuss the application of the amorphous mixture solids to pharmaceutical formulations.

* To whom correspondence should be addressed. e-mail: izutsu@nihs.go.jp

Experimental

Materials 1,3-Diaminopropane was purchased from Kanto Kagaku Kogyo Co. (Tokyo, Japan). 1,3-Diamino-2-hydroxypropane was the product of Sigma-Aldrich Inc. (St. Louis, MO, U.S.A.). Tricarballic acid was obtained from Alfa Aesar GmbH & Co. KG (Karlsruhe, Germany). DL-Malic acid, D-(+)-malic acid, glycolic acid, L-(+)-tartaric acid, glutaric acid, adipic acid, DL-lactic acid (2-hydroxypropanoic acid), 1-aminopropane (propylamine), 1,4-diaminobutane, 1,6-diaminohexane, 1,8-diaminooctane, and other reagents were of analytical grade obtained from Wako Pure Chemical Industries Co. (Osaka, Japan).

Thermal Analysis Thermal analysis of frozen solutions and freeze-dried solids was conducted with a differential scanning calorimeter (DSC Q-10, TA Instruments, New Castle, DE, U.S.A.) with Universal Analysis 2000 software (TA Instruments). An aliquot (10 μ l) of aqueous solution in an aluminum cell was cooled to -70°C at $10^\circ\text{C}/\text{min}$ and then scanned at $5^\circ\text{C}/\text{min}$. Freeze-dried solids (1–2 mg) in hermetic aluminum cells were scanned from -30°C at $5^\circ\text{C}/\text{min}$ under nitrogen flow. Physical mixtures containing 1,3-diamino-2-hydroxypropane and citric acid (1.5–2.5 mg) in aluminum cells were melted at 165°C for 3 min and then cooled rapidly by immersion in liquid nitrogen to prepare quench-cooled melt solids. The cells were transferred to the furnace of the calorimeter at 15°C and then scanned from -50°C at $5^\circ\text{C}/\text{min}$ to obtain the glass transition temperatures. Glass transition temperatures were determined as the maximum inflection point of the discontinuities in the heat flow curves.

Freeze-Drying A freeze-drier (Freezone-6, Labconco, Kansas City, MO, U.S.A.) equipped with temperature-controlling trays was used for lyophilization. Aqueous solutions containing the solutes (total 200 mM, 300 μ l) in flat-bottom glass vials (13 mm diameter) were placed on the shelf of the freeze-drier at room temperature. The shelf was cooled to -40°C at $0.5^\circ\text{C}/\text{min}$ and then maintained at that temperature for 2 h before drying. The frozen solutions were dried under vacuum (21 mTorr) maintaining the shelf temperature at -40°C for 15 h, -30°C for 6 h, and 35°C for 6 h. The shelf was heated at $0.2^\circ\text{C}/\text{min}$ between the drying steps. The vials were closed with rubber stoppers under the vacuum. Solids for near-infrared analysis were prepared by freeze-drying the aqueous solutions (1 ml) in larger vials (18 mm diameter).

Mid- and Near-Infrared Spectroscopy (IR, NIR) An FT-IR spectrophotometer (MB104, ABB Bomen, Quebec, Canada) and GRAMS/32 software (Galactic Ind. Co., Salem, NH, U.S.A.) were used to obtain mid-infrared spectra of the solids (approx. 1 mg sample solid) in a pressed potassium bromide disk (approx. 250 mg). Transition spectra of the sample disks were obtained at 4 cm^{-1} resolution in 128 scans. Near-infrared spectroscopy was performed by using a Bruker MPA system with a diffuse-reflectance integrating-sphere probe (PbS detector) and OPUS software (Ettingen, Germany). Near-infrared light was directed upward from the bottom of the glass vials containing freeze-dried solids to obtain the reflected signal over a range of $4000\text{--}12000\text{ cm}^{-1}$ with a resolution of 4 cm^{-1} in 128 scans.

Powder X-Ray Diffraction (XRD) and Residual Water Content Measurement The powder X-ray diffraction patterns were measured at room temperature with a Rint-Altima diffractometer (Rigaku, Tokyo, Japan) with $\text{CuK}\alpha$ radiation at $40\text{ kV}/40\text{ mA}$. The samples were scanned in the area of $5^\circ < 2\theta < 35^\circ$ at an angle speed of $5^\circ/\text{min}$. An AQP-6 volumetric titrator (Hiranuma Sangyo, Ibaraki, Japan) was used to determine the amount of water in the freeze-dried solids suspended in dehydrated methanol by the Karl-Fischer method.

Results

Figure 1 shows thermograms of frozen aqueous solutions containing a carboxylic acid and an amine (200 mM). The structure of the chemicals used in this study and their physical properties in the frozen solutions obtained by thermal analysis are summarized in Table 1. Some solutes showed intrinsic propensities to crystallize in the freeze-concentrated phases. An endotherm (-15.8°C) in a frozen malonic acid solution suggested melting of the eutectic crystal. The exotherm (-53.1°C) and endotherm (-19.3°C) peaks

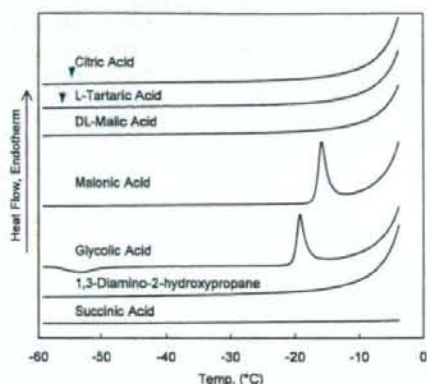


Fig. 1. Thermograms of Frozen Solutions Containing a Carboxylic Acid or an Amine (200 mM)

Aliquots (10 μ l) of solutions in hermetic aluminum cells were scanned from -70°C at $5^\circ\text{C}/\text{min}$. Arrowheads denote the glass transition of maximally freeze-concentrated solutes (T_g').

Table 1. Structure and Thermal Property of Carboxylic Acids and Amines in Frozen Aqueous Solutions Obtained by Thermal Analysis

| | MW | Functional groups | | | Property in frozen solutions | |
|------------------------------|-------|-------------------|----|-----------------|------------------------------|------------------------------|
| | | COOH | OH | NH ₂ | Crystallinity | Thermogram |
| Acetic acid | 60.1 | 1 | 0 | 0 | Crystallized | Endotherm |
| Glycolic acid | 76.1 | 1 | 1 | 0 | Crystallized | Exotherm/endotherm |
| DL-Lactic acid | 90.1 | 1 | 1 | 0 | Amorphous | $T_g' < -60^\circ\text{C}$ |
| Malonic acid | 104.1 | 2 | 0 | 0 | Crystallized | Endotherm |
| Succinic acid | 118.1 | 2 | 0 | 0 | Crystallized | Flat |
| Glutaric acid | 132.1 | 2 | 0 | 0 | Crystallized | Flat |
| Adipic acid | 146.1 | 2 | 0 | 0 | Crystallized | Exotherm |
| Pimelic acid | 160.2 | 2 | 0 | 0 | Crystallized | Flat |
| L-Malic acid | 134.1 | 2 | 1 | 0 | Amorphous | $T_g' < -60^\circ\text{C}$ |
| L-Tartaric acid | 150.1 | 2 | 2 | 0 | Amorphous | $T_g' : -57.1^\circ\text{C}$ |
| Tricarballic acid | 176.1 | 3 | 0 | 0 | Amorphous | $T_g' : -52.1^\circ\text{C}$ |
| Citric acid | 192.1 | 3 | 1 | 0 | Amorphous | $T_g' : -55.1^\circ\text{C}$ |
| 1-Aminopropane | 59.1 | 0 | 0 | 1 | Crystallized | Endotherm |
| 3-Amino-1-propanol | 75.1 | 0 | 1 | 1 | Amorphous | $T_g' < -60^\circ\text{C}$ |
| 1,3-Diaminopropane | 74.1 | 0 | 0 | 2 | Amorphous | $T_g' < -60^\circ\text{C}$ |
| 1,4-Diaminobutane | 88.2 | 0 | 0 | 2 | Crystallized | Endotherm |
| 1,6-Diaminohexane | 116.2 | 0 | 0 | 2 | Crystallized | Endotherm |
| 1,8-Diaminooctane | 144.3 | 0 | 0 | 2 | Crystallized | Flat |
| 1,3-Diamino-2-hydroxypropane | 90.1 | 0 | 1 | 2 | Amorphous | $T_g' < -60^\circ\text{C}$ |

observed in a heating scan of a frozen glycolic acid solution indicated eutectic crystallization and subsequent melting, respectively. The flat thermogram of a frozen succinic acid solution up to the ice-melting temperature suggested crystallized solutes. Some of these frozen solutions showed an exotherm that indicated eutectic crystallization in the cooling process before the thermal scan (data not shown). L-Tartaric acid and citric acid remained amorphous in the freeze-concentrated phase, presenting glass transition of the maximally freeze-concentrated solute phase (T_g') at -55.1°C and -57.1°C , respectively.⁷ The absence of particular thermal transitions and the gradual shift of the thermogram in some other single-solute frozen solutions (e.g., DL-malic acid, 1,3-diamino-2-hydroxypropane) suggested that T_g' transition of the amorphous concentrated phase occurred at temperatures below the measurement temperature range ($< -60^\circ\text{C}$).

Figures 2 and 3 show T_g' of frozen binary solutions containing various diamines and L-tartaric acid or citric acid. Most of the solute combinations showed a bell-shaped profile of T_g' that depended largely on the number of functional groups in the amines. Frozen mixture solutions containing amines and citric acid showed the T_g' peaks at lower acid molar ratios than in the combination with L-tartaric acid. Transition temperatures (T_g') of frozen solutions containing the acids and various diamines were significantly higher than those of the mixtures with monoamines (e.g., 1-amino-propane). Slightly higher transition temperatures of the frozen solutions containing citric acid and 1,8-diaminooctane compared to those with smaller alkyldiamines (e.g., 1,3-diaminopropane) indicated a relatively small effect of the component molecular size on the T_g' of the mixture phases. Introduction of hydroxyl groups to a diamine (e.g., 1,3-diaminopropane to 1,3-diamino-2-hydroxypropane) raised the T_g' of the frozen mixture solutions to some extent. Mixing with L-tartaric acid or citric acid prevented crystallization of some amines (e.g., 1,4-diaminobutane) in the frozen solutions. In contrast, some frozen mixture solutions showed thermal peaks that suggested crystallization of the salts. For example, a frozen solution containing 60 mM diaminooctane and 140 mM L-tartaric acid showed a T_g' (-32.7°C) and a eutectic crystallization exotherm peak (-19.9°C) in a thermal scan (data not shown).

Mixing of 1,3-diamino-2-hydroxypropane and some carboxylic acids (e.g., succinic acid) also induced a significant upward shift of the T_g' (Fig. 4). The transition temperatures depended largely on the compositions of the carboxyl and hydroxyl groups in the acids. Most of the frozen mixture solutions showed the highest T_g' at the solute concentration ratios relatively rich in carboxylic acid. Alkyl chain length of the dicarboxylic acids gave limited effects on the T_g' of the mixture frozen solutions. DL-Malic acid and D-malic acid presented virtually identical T_g' profiles of the mixture frozen solutions. Mixing with 1,3-diamino-2-hydroxypropane prevented crystallization of some dicarboxylic acids (e.g., malonic acid, pimeric acid) in the frozen solutions (data not shown). High T_g' of the frozen solutions containing 1,3-diamino-2-hydroxypropane and the hydroxy carboxylic acids (DL-malic acid, L-tartaric acid, citric acid) indicated a large effect of the hydroxyl group in reducing the component mobility in the freeze-concentrated phase. Frozen solutions containing 1,3-diamino-2-hydroxypropane and acetic acid or

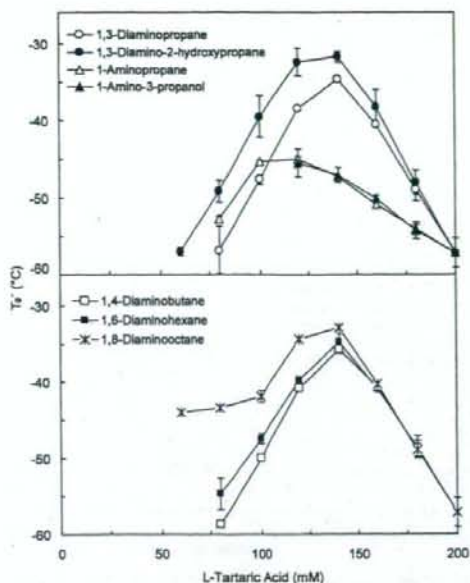


Fig. 2. Glass Transition Temperatures of the Maximally Freeze-Concentrated Phase (T_g') of Frozen Aqueous Solutions Containing L-Tartaric Acid and Various Amines

Frozen solutions (10 μl , 200 mM total) were scanned from -70°C at $5^\circ\text{C}/\text{min}$ ($n=3$).

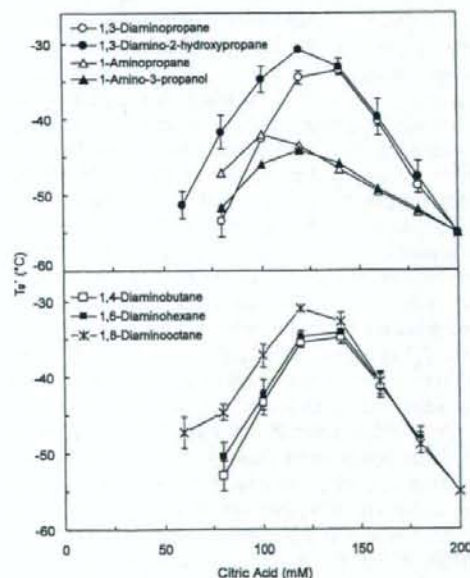


Fig. 3. Glass Transition Temperatures of the Maximally Freeze-Concentrated Phase (T_g') of Frozen Aqueous Solutions Containing Citric Acid and Various Amines

Frozen solutions (10 μl , 200 mM total) were scanned from -70°C at $5^\circ\text{C}/\text{min}$ (average \pm S.D., $n=3$).

glycolic acid showed a gradual shift of the thermograms that suggested an amorphous mixture freeze-concentrated phase with T_g' below the measurement temperature range ($< -60^\circ\text{C}$) (data not shown). The absence of apparent thermal transitions in frozen solutions containing some dicarboxylic